Astron. Astrophys. 291, L5–L8 (1994)

ASTRONOMY AND ASTROPHYSICS

Letter to the Editor

Dust emission of galactic cirrus from DIRBE observations

J.P. Bernard[1,2], F. Boulanger[2], F.X. Désert[2], M. Giard[3], G. Helou[1], and J.L. Puget[2]

[1] Infrared Processing and Analysis Center, California Institute of Technology, MS 100-22, Pasadena CA 91125, USA
[2] Institut d'Astrophysique Spatiale, bât. 121, Université Paris XI, F-91405 Orsay Cedex, France
[3] Centre d'Etude Spatiale du Rayonnement, 9 avenue du Colonel Roche, BP 4346, F-31029 Toulouse Cedex, France

Received 5 April 1994 / Accepted 30 June 1994

Abstract.

We present the spectral distribution of dust in the diffuse ISM as derived from the first release of the DIRBE (Diffuse Infrared Background Explorer) data, in the wavelength range from 3.5 to 240 μm. Although the spectrum of diffuse regions strongly decreases from 12 μm toward shorter wavelengths, it is found that some dust emission is still present in the L and M bands. On average, it corresponds to $\simeq 1\%$ of the total IR emission. The comparison with the 3.3 μm Polycyclic Aromatic Hydrocarbon (PAH) feature emissivity of the diffuse medium in the inner galaxy shows that only a small fraction $(8-16\%)$ of the DIRBE L band ISM emission is likely to be produced by the 3.3 μm feature. Along with the presence of an important dust emission in the DIRBE M band, where no PAH feature is expected, this implies that a continuum component and/or other features from dust also contribute significantly to the short wavelength emission. The carrier of this emission still has to be identified. Large color variations are observed from region to region over most of the DIRBE range, which might reflect abundance variations of the various dust components.

Key words: ISM:clouds – ISM:dust,extinction – ISM:molecules – Infrared:interstellar:continuum

1. Introduction

The diffuse IR emission of galactic interstellar matter has been first evidenced in the IRAS (Infrared Astronomical Satellite) data at 100 μm (Hauser et al. 1984) and appears as a series of complex filamentary structures (the so-called cirrus clouds) extending away from the galactic plane (Low et al. 1984). The cirrus spectrum rises from 60 to 100 μm and shows up unexpectedly in the 12 and 25 μm IRAS bands (Boulanger et al. 1985). It has become increasingly clear that this spectrum requires emission of transiently heated small dust particles to produce the short wavelength excess, along with colder classical size grains, whose peak emission lies above 100 μm. Although the nature of the small particles is still a controversial issue, it has been argued that PAH molecules (Léger and Puget 1984) could be responsible for the 12 μm excess as well as for the 3.3 μm and other features observed in emission. The sensitivity of ground-based observations allows detection of the PAH feature only in regions with high UV radiation densities (e.g., HII regions/ molecular cloud interfaces, reflection and planetary nebulae, ...). In these regions, standard grains are also much hotter than in cirrus clouds, so that the 12-25 μm excess is less obvious. The 3.3 μm feature emission along the galactic plane was recently mapped using the AROME balloon experiment (Giard et al. 1988). However, no detection of the PAH feature toward unconfused cirrus clouds has ever been performed. Therefore, no direct observational evidence is available up to now to attribute the NIR and IR emission to the 3.3 μm carriers.

In this letter, we present galactic maps of the dust emission obtained using the DIRBE instrument on board the COBE [1] (Cosmological Background Explorer) satellite, which evidence for the first time the cirrus emission at wavelengths shorter and longer than the IRAS coverage, including in the L band which contains the PAH 3.3 μm feature.

2. Data Analysis

During Dec 1989 to June 1990, the DIRBE instrument performed a high sensitivity mapping of the whole sky with an angular resolution of 0.7°, in ten infrared photometric bands ranging from 1.25 to 240 μm, four of which closely match those of the IRAS satellite. Instrument characteristics and performance have been described by Hauser et al. (1991) and Boggess et al. (1992). We used the first release of the data, which gathers observations along the galactic plane ($|b| < 15°$ for $30° < l < 330°$ and $|b| < 10°$ elsewhere), interpolated to a constant solar elongation of 90° (DIRBE explanatory supplement 1993), to study the dust emission in this wavelength range. These maps show that the large scale emission in the range $1.25 < \lambda < 4.9$ μm is dominated by stellar emission from the galactic disk and bulge and is heavily obscured near the plane, especially toward the inner galactic regions. The stellar emission distribution and colors in these maps have been studied in some detail by Arendt et al. (1994) and Weiland et al. (1994), and is dominated by late K and M giant stars in the galactic disk and halo. At longer wavelengths, the maps are strongly affected by thermal emission from hot dust in the zodiacal cloud (e.g. Berriman et al. 1994), which was also obvious in the IRAS data. In order to bring out the galactic dust emission, both the stellar and the zodiacal components have to be subtracted from the maps.

[1] COBE is supported by NASA's Astrophysics Division

2.1. Zodiacal light removal

We compared the DIRBE maps at 12 and 25 μm with the predictions of the Zodiacal Light (ZL) emission model presented in Wheelock et al. (1994). The free parameters of this physical model (dust emissivity and temperature distribution, cloud orientation) were originally optimized to reproduce the ZL emission in the IRAS data. The model predictions were calculated for each DIRBE data point, taking into account the Earth position along its orbit at the time of the year the data were recorded and the line of sight direction through the zodiacal dust cloud. The use of such a model allowed us to account for the dependence of the ZL emission on ecliptic longitude and latitude (λ, β). We compared the predictions of the model with the DIRBE data in two windows (hereafter the $|b| = 9°$ windows) taken in the highest latitude range within the released DIRBE data: ($10° < \lambda < 190°$, $8° < |b| < 10°$) and ($\lambda < 10°$ or $\lambda > 190°$, $8° < |b| < 10°$). The distinction of two ecliptic longitude ranges is made necessary by the two steps in sky brightness which result from making maps at a fixed solar elongation (DIRBE explanatory supplement 1993). It was found that the model generally underestimates and overestimates the ZL emission in the first and second ecliptic longitude range respectively. At 12 μm, these differences correspond to $\simeq$ 2.5 MJy/sr (10 %) and $\simeq$ 4.5 MJy/sr (18 %) respectively in the ecliptic plane. In addition, some smaller scale structures appear in the data such as the zodiacal bands at $\beta \simeq \pm 9°$, which are not accounted for by the model. An average correction profile was generated by fitting a lower envelope (lowest 10^{th} percentile in $\Delta\beta = 1°$) to the ecliptic latitude profile of the difference data-model in the $|b| = 9°$ windows. It was assumed that the component varying with β is entirely due to the ZL. After correction, the residual difference is < 3% (mainly due to slightly different profiles between $b = 9°$ and $-9°$), which is regarded as the accuracy of the ZL subtraction at 12 and 25 μm in the range $|b| < 10°$.

At $\lambda > 25\,\mu$m, no similar correction was possible because galactic emission dominates everywhere in the region covered by the first release of the DIRBE data. At 60 and 100 μm, we adopted the predictions of the ZL model corrected for the DIRBE-IRAS calibration differences (see DIRBE explanatory supplement 1993). The zero level of the ZL in all IRAS bands was set so that ZL subtracted brightness at $|b| = 10°$ match those derived by Boulanger & Pérault (1988). No ZL was subtracted from the 140 and 240 μm maps. In the 4.9 μm channel, ZL emission is still essentially thermal and a similar procedure was adopted, but the correction was computed in the $|b| = 9°$ window toward the anticenter, where star light does not dominate the total brightness. In the range $1.25 < \lambda < 4.9\,\mu$m, some ZL contribution can still be seen in the $|b| = 9°$ anticenter window, where the ecliptic crosses the galactic plane. The ecliptic latitude profile measured in this window was fitted with the analytical function proposed by Hauser (1993). The ZL intensity has its minimum in the L band and the FWHM of the ecliptic latitude profiles increases by a factor of two from 3.5 μm to 4.9 μm. This is consistent with emission at $\lambda < 3.5$ and $\lambda > 3.5\,\mu$m being due to strongly forward scattering and thermal emission respectively. Note that the procedure described above artificially subtracts any constant or slowly varying galactic component. However, the results discussed in Sect. 3 are based on small scale variations of the intensity and therefore are unsensitive to this problem. Future studies based on the complete set of DIRBE data will probably allow one to construct more comprehensive physical models of the ZL emission.

2.2. Stellar emission removal

The diffuse stellar components from the galactic bulge and disk were isolated following the method proposed by Arendt et al. (1994). Images in the two shorter wavelength bands (1.25 and 2.2 μm) are assumed to contain only stellar emission and are used to derive $\tau_{1.25}$, the optical depth at 1.25 μm, by solving:

$$(I^*_\lambda/I^*_{1.25})_{\rm int} = I^*_\lambda e^{\tau_\lambda}/I^*_{1.25}e^{\tau_{1.25}}, \quad (1)$$

for $\lambda = 2.2\,\mu$m, where I^*_λ denotes the DIRBE maps at wavelength λ, $(I^*_\lambda/I^*_{1.25})_{\rm int}$ is the intrinsic color of the stellar component and $\tau_\lambda/\tau_{1.25}$ was taken from the NIR extinction curve derived by Rieke and Lebofsky (1985). The extinction corrected stellar contribution is then calculated at each NIR wavelength by solving Eq. 1 for I^*_λ. The intrinsic colors adopted (1, 1.7 and 2.1 for $(I^*_{1.25}/I^*_{2.2})_{\rm int}$, $(I^*_{2.2}/I^*_{3.5})_{\rm int}$ and $(I^*_{3.5}/I^*_{4.9})_{\rm int}$ respectively) were derived in regions with low extinction and low dust emission, where the background is dominated by the stellar emission. They are consistent with the values derived by Arendt et al. The diffuse stellar emission maps obtained show a smooth distribution where contributions from the galactic bulge and disk can clearly be distinguished.

Equation 1 assumes that most of the stellar emission is located in the background of the dust clouds. As we are specifically interested in close cirrus at intermediate latitude and the scale height of the K and M giants ($\simeq$ 475 pc e.g. Robin and Crézé 1985) is larger than that of galactic clouds ($\simeq$ 100 pc), this assumption was preferred to a homogeneous mixture of dust and stars. The procedure also assumes that a similar stellar distribution is seen at all wavelengths. This is not valid in high extinction regions toward the inner galaxy where the stellar density strongly varies with galactic radius and the depth sampled along a given line of sight increases with wavelength.

3. Results and discussion

In Fig. 1, we present the maps of the dust emission obtained in the L (3.5 μm), 12 and 240 μm bands as well as for $\tau_{1.25}$. A low spatial frequency background (lowest 20^{th} percentile level in $\Delta l \times \Delta b = 50° \times 2°$ around each pixel) was subtracted from each map, in order to remove the galactic gradient along l and to make it easier to isolate individual structures. Unfiltered 240 μm and $\tau_{1.25}$ maps were previously presented by Sodroski et al. (1994) and Arendt et al. (1994) respectively. In the L(3.5 μm) and M (4.9 μm) bands, the galactic plane appears as a narrow band in the range $-70° < l < 50°$, $|b| < 3°$. At a scale of a few degrees along the galactic plane, they show a structure closely similar to the 3.3 μm feature map measured by the AROME balloon experiment (Giard et al. 1994, see below). In addition to the inner galaxy, several regions have significant emission in the L and M bands as the Cygnus complex ($l \simeq 80°$) and the Cepheus and Perseus region ($95° < l < 150°$).

3.1. Spectrum of diffuse regions

In order to determine the typical spectrum of the dust emission in intermediate latitude diffuse regions in an unbiased way, the selected clouds were identified at 240 μm in $4° < b < 6°$ and

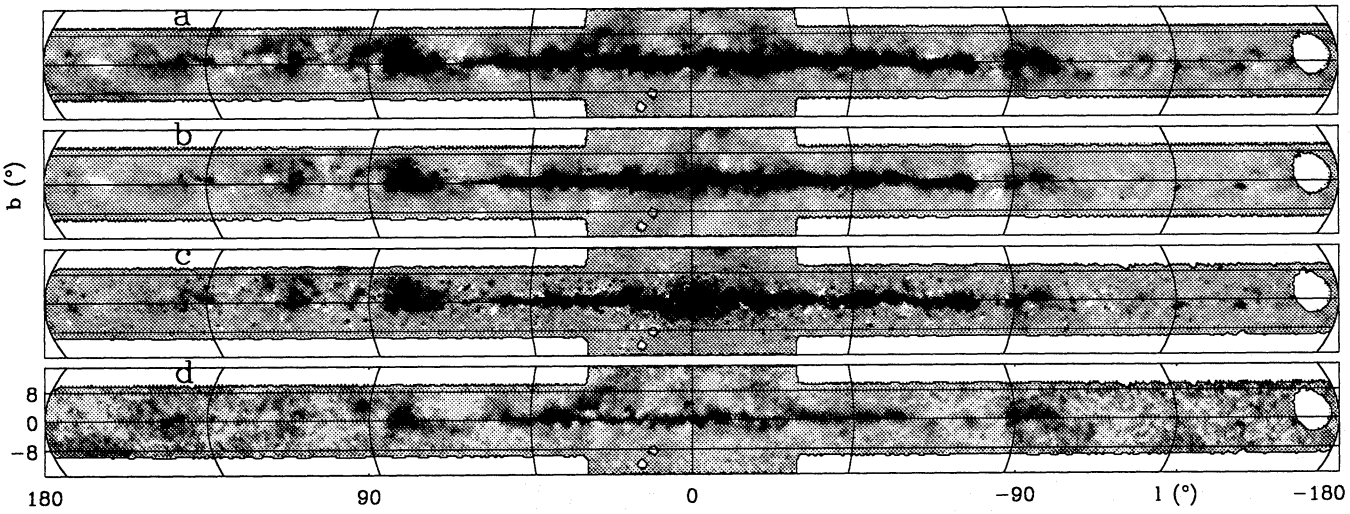

Fig. 1. Filtered maps of the dust emission at 240 (a), 12 (b), 3.5 μm (c) and $\tau_{1.25}$ (d) derived as described in Sect. 2. The black areas correspond to values larger than 120, 4 and 0.2 MJy/sr for intensity maps respectively and $\tau_{1.25} > 1$.

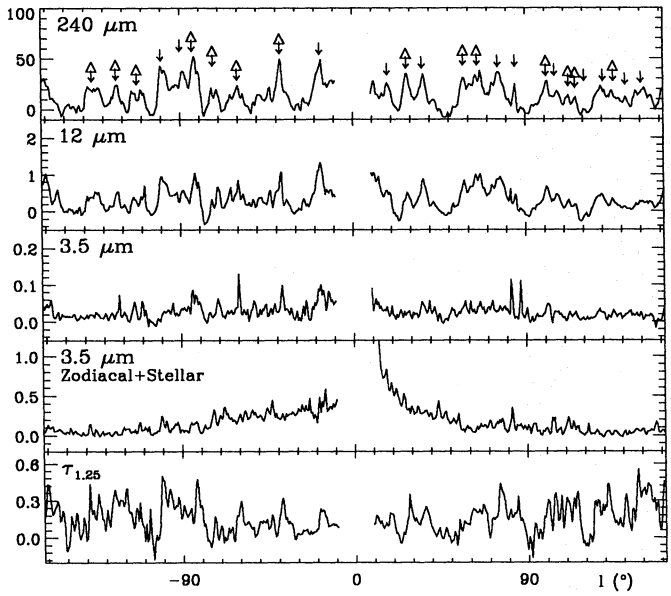

Fig. 2. Filtered profiles averaged in $-6° < b < -4°$ for the dust emission at 240, 12 and 3.5 μm (MJy/sr), ZL and starlight contribution at 3.5 μm (MJy/sr) and $\tau_{1.25}$. The clouds selected to compute the average spectrum of Fig. 3 are shown by triangles.

$-6° < b < -4°$ in the maps of Fig. 1. One of the averaged cuts used is shown in Fig. 2. The region $|l| < 10°$ is affected by defects at 3.5 and 4.9 μm caused by the stellar subtraction in the bulge and was disregarded. The spectrum of the individual regions was then determined by integrating into the 2D maps of the filtered dust emission from 3.5 μm to 240 μm in a region with $|b| > 4°$ and above the 240 μm contour corresponding to the half peak brightness of each structure. For each individual region, a background was fitted by a low degree polynomial surface constrained in a region surrounding the 240 μm contour and was subtracted. Pixels that might be affected by emission from known IR point sources were identified by comparison to the IRAS PSC and disregarded. For each cloud, the error due to background subtraction was estimated by modifying the degree of the polynomial surface used in the subtraction. Errors caused by the stellar background removal were also estimated, assuming an rms error $\Delta\tau_{1.25} \simeq 0.37\tau_{1.25}$ derived from the $\tau_{1.25}$ vs τ_{240} correlation presented by Arendt et al. 1994. However, this last contribution is generally small (< 10%) and the overall uncertainty ($\sigma(\lambda)$) is dominated by the background subtraction for most structures. Most of the selected clouds show significant emission at all wavelengths. They also exhibit strong color variations (compare cuts shown in Fig. 2, for instance, the clouds at $l \simeq -110°$ and $-123°$) over most of the spectral range. These variations are particularly strong in the L and M bands and exceed the error from both stellar and ZL subtraction. However, no simple correlation could be evidenced between the NIR and longer wavelength parts of the spectra.

The average spectrum for the diffuse medium at $|b| = 5°$ is shown in Fig. 3. The sample includes the individual regions in $4° < |b| < 6°$ with the lowest equilibrium temperature of big grains ($T_{BG} < 20K$) and showing significant emission at all wavelengths. The temperature threshold eliminates the clouds in bright regions such as CygnusX, which may not be relevant to the average diffuse medium. T_{BG} was derived by fitting the 100, 140 and 240 μm bands with a $\lambda^{-1.5}$ emissivity grey body. It is found to vary from 15 to 23 K. The spectra of the selected clouds (22 in total) were normalized to their total energy and averaged using a weight $\omega_i \propto 1/(\sum_\lambda \sigma_i(\lambda)/I_\lambda)^2$. The error bar in the figure is the standard deviation in the sample and is representative of the average color dispersion of the selected clouds. Individual clouds with a spectrum significantly different from that of Fig. 3 probably exist, but at this stage we are unable to provide any information about the probability distribution of the colors. The average energy in the L and M bands normalized to the 12 μm brightness is $(\Delta\lambda I_\lambda)_L/(\lambda I_\lambda)_{12} = (7.1 \pm 1.6)\ 10^{-2}$ and $(\Delta\lambda I_\lambda)_M/(\lambda I_\lambda)_{12} = (2.4 \pm 0.7)\ 10^{-2}$ respectively. The average 12/100 ratio is $(\lambda I_\lambda)_{12}/(\lambda I_\lambda)_{100} = (4.1 \pm 0.9)\ 10^{-1}$. Figure 3 also plots the predictions of the model by Désert et al. (1990) for the solar neighborhood. Although the predicted colors are in general agreement with those observed, the model tends to

overestimate the brightness in the L and M bands. The difference in the 100 μm band is mainly due to the gain difference between the DIRBE and the IRAS data. Adjustment of the model to the DIRBE calibration is necessary and will be addressed in a subsequent publication.

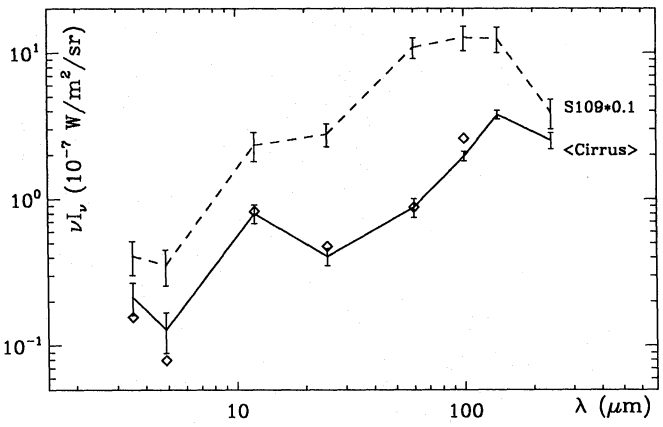

Fig. 3. Average spectrum (solid line) for the cold diffuse medium at $|b| = 5°$. The scaling corresponds to $\simeq 10^{21}$ H/cm^2. The spectrum of the HII region S109 in CygnusX (dash) and that proposed by Désert et al. for the solar neighborhood (diamonds) are shown for comparison.

3.2. Comparison with the AROME 3.3 μm feature data

The AROME balloon borne experiment measured the intensity of the galactic 3.3 μm feature (see Giard et al. 1988). Here, we use those data in order to assess the contribution of the feature to the interstellar emission detected in the DIRBE L band toward the galactic plane.

In order to check the consistency of AROME and DIRBE calibrations, we averaged data over the longitude range $10° < l < 30°$, to produce a mean cut of the continuum emission across the galactic plane. The DIRBE L band includes wavelengths from $\lambda = 3.0$ to 4.0 μm, whereas the AROME continuum band covers a slightly smaller spectral range from $\lambda = 2.8$ to 3.7 μm, with a low transmission region around 3.3 μm ($\Delta\lambda = 0.16$ μm), corresponding to the interstellar emission feature. For both data, the emission is completely dominated by that of stars. Thus, the slight difference in the spectral range will only induce a minor difference between the two datasets. The AROME data is made of scans across the plane, which are flattened to a zero brightness at $|b| > 3°$ to remove instrumental drifts. To compare the two datasets we fitted a similar baseline to the DIRBE cut. As for the AROME data, this fit is made with a polynomial of degree 3 over $3° < |b| < 5°$. After baseline subtraction, the two profiles agree within 5%, which is within the calibration uncertainty of the AROME instrument.

For the diffuse medium, Giard et al. (1994) have shown that the variations of the 3.3 μm feature to IRAS 12 μm ratio observed toward the inner Galaxy can all be attributed to extinction effects. They derive an average value for this ratio of $(8.2 \pm 0.8)\ 10^{-3}$, independant of the galactocentric distance. The mean L to 12 μm color of the interstellar regions selected in this paper is $(7.1 \pm 1.6)\ 10^{-2}$. Consequently, the contribution of the 3.3 μm feature to the interstellar L band emission is only $R \simeq 8 - 16\%$. Note that to do this comparison we have combined the emission ratio measured in the plane for molecular ring material with one measured for more nearby matter at a few degrees from the plane. The quoted contribution relies on the assumption that the two emission ratios do not vary significantly with galactocentric distance.

The small contribution of the 3.3 μm feature implies that most of the interstellar excess observed in the DIRBE L band is due to a continuum and/or to emission features which do not peak at 3.3 μm. If we assume that the spectral shape of the 3.3 μm feature in the diffuse galactic emission is identical to the one measured on the Orion bar by Sellgren et al. (1990), the comparison of the AROME and DIRBE observations imply that the feature is superposed on a strong continuum with a feature to continuum contrast $I_\lambda(3.3\,\mu m)/I_\lambda^{cont}(3.3\,\mu m) \simeq 2.4$. This value is lower than for Orion or reflection nebulae (in the range 8 to 13: Sellgren et al. 1985, 1990) and falls in the range of what is observed for Planetary Nebulae (e.g. Russell et al. 1977). The presence of this near infrared interstellar continuum emission is also supported by the detection of the interstellar excess in the DIRBE M band where no strong feature is expected. For the continuum alone, the L to M color derived for the 5° cirrus is $I_\lambda^{cont}(3.5\,\mu m)/I_\lambda^{cont}(4.9\,\mu m) \simeq 2.1$, a value consistant with the color (2 to 2.3) derived by Sellgren et al. (1985) toward reflection nebulae.

Acknowledgements. We are grateful to the Goddard Space Flight Center team for their help in reducing the DIRBE data. J.P. Bernard acknowledges financial support from the European Space Agency during the completion of this study.

References

Arendt R. G. et al., 1994, ApJ 425, L85.
Berriman G.B. et al., 1994, ApJ 431, Lxx.
Boulanger F., Baud B., van Albada G.D., 1985 A&A 144, L9.
Boulanger F., Pérault M., 1988 ApJ 330, 964.
Boggess et al., 1992, ApJ 397, 420.
Désert F-X., Boulanger F., Puget J.L., 1990, A&A 237 215.
DIRBE explanatory supplement, 1993, version 19 July 1993, distributed by National Space Science Data Center.
Giard M. et al., 1988, A&A 201, L1.
Giard M. et al., 1994, A&A 286, 203.
Hauser et al., 1984, ApJ 278, L11.
Hauser et al. 1991 in "After the First Three Minutes", Eds S.S. Holt, C.L. Bennett, V. Trimble, AIP Conf. Proc., p48.
Hauser M.G. 1993 in AIP Conf. Proc. 278, "Back to the Galaxy", eds S.S. Holt, F. Verter.
Léger A., Puget J.L., 1984, A&A 137, L5.
Low F.J. et al. 1984, ApJ 278, L19.
Rieke G.H., Lebofsky M.J., 1985, ApJ 288, 618.
Robin A., Crézé M., 1986, A&A 157, 71.
Rusell R.W., Soifer B.T., Merrill K.M., 1977, ApJ 213, 66.
Sellgren K. et al. 1985, ApJ, 299, 416.
Sellgren K., Tokunaga A.T., Nakada Y., 1990, ApJ 349, 120.
Sodroski T.J. et al. 1994, ApJ 428, 638.
Wheelock S.L. et al., 1994 IRAS Sky Survey Atlas explanatory supplement, JPL publication 94-11 (Pasadena:JPL).
Weiland J.L. et al., 1994, ApJ 425, L81.

This article was processed by the author using Springer-Verlag LaTeX A&A style file 1990.